Complexity Analysis of Three-dimensional Stochastic Discrete Fracture Networks with Fractal and Multifractal Techniques

Weiwei Zhu[a], Xupeng He[b], Gang Lei[c], Moran Wang[a,*]

[a] *Department of Engineering Mechanics, Tsinghua University, Beijing, China*
[b] *Ali I. Al-Naimi Petroleum Engineering Research Center (ANPERC), King Abdullah University of Science and Technology, Thuwal, KSA*
[c] *Faculty of Engineering, China University of Geosciences, Wuhan, China*

Abstract

The fractal dimension and multifractal spectrum can characterize the complexity of fracture sets. However, studies of impacts of fracture geometries on their fractal and multifractal characteristics are largely insufficient, especially for three-dimensional (3-D) fracture networks (natural fractures are always 3-D instead of 2-D). In this work, we construct 3-D stochastic discrete fracture networks with an open-source DFN software, HatchFrac. Systematical investigations are then conducted to study the impact of geometrical fracture properties and system sizes on the fractal and multifractal characteristics. The box-counting method is adopted to calculate the fractal dimension and multifractal descriptors. The fractal dimension, D, and the difference of the singularity exponent, $\Delta\alpha$, represent the fractal and multifractal patterns, respectively. Two critical (percolative and over-percolative) stages of fracture networks are considered. 3-D fracture networks share similar characteristics with 2-D fracture networks at percolation. However, results at an over-percolative stage are systematically different. At the first stage, fracture orientations (κ), lengths (a) and system sizes (L) have positive correlations with D and $\Delta\alpha$. D is weakly correlated with fracture positions (F_D), meaning that the fractal dimension is

*Moran Wang
Email address: mrwang@tsinghua.edu.cn (Moran Wang)

insensitive to clustering effects. However, $\Delta\alpha$ is strongly correlated with F_D, implying that $\Delta\alpha$ can characterize the heterogeneity caused by clustering effects. a and L are positively correlated with $\Delta\alpha$, and κ and F_D have negative correlations. At stage two, the sensitivity results on D are similar to stage one, but a and L become negatively correlated with $\Delta\alpha$. Impacts of κ and F_D become more significant.

Keywords: Fractal; Multifractal; Complexity; Heterogeneity; Stochastic discrete fracture networks;

1. Introduction

Fractures are pervasive in crustal rocks and usually form complicated networks. Partially open or stimulated fractures typically have a much higher permeability than the surrounding matrix, which makes fracture networks essential in many fluid transportation problems in the subsurface (Berkowitz, 2002; Follin et al., 2014; Pérez-Flores et al., 2017; He et al., 2021). Similar fracture network patterns are observable in different scales, from millimeters (Wu et al., 2019) to kilometers (Aviles et al., 1987). Therefore, natural fractures are usually regarded as self-similar sets (Otsuki and Dilov, 2005; Shi et al., 2018).

Fractal and multifractal theory (Mandelbrot, 1977, 1982) is used to characterize the complexity of irregular sets regardless of the scales. The complexity of fracture networks refers to two main aspects. One is the spatial coverage and can be characterized by the fractal dimension. A larger fractal dimension represents better spatial coverage. The other aspect of complexity is the heterogeneity of the fracture network. The heterogeneity of fracture networks can be observed from fracture data in different dimensions. For 1-D fracture data, such as scanline sampling and borehole images, fracture spacing (Priest and Hudson, 1976) can quantify space variations of fractures, but information on the fracture length and interaction between fractures are unavailable. For 2-D fracture data, such outcrop observations, fracture intensity (Dershowitz et al., 1992) or graph representation (Prabhakaran et al., 2021) can provide more information on the

fracture arrangements and variations. However, quantifying and evaluating the heterogeneity is nontrivial. Variations of the 2-D fracture intensities can represent the heterogeneity, but this descriptor is sensitive to the grid size of the domain partition. Different fracture geometrical properties can cause the heterogeneity of fracture networks, such as fracture length, orientations, positions of fracture centers. Without quantifying the heterogeneity, the separation of impacts from different fracture geometries is impossible. Alternately, in multifractal theory, the target set is regarded as a collection of fractal subsets, and each subset can be characterized by a specific fractal dimension, which in turn yields a multifractal spectrum (Berkowitz and Hadad, 1997). The multifractal spectrum provides abundant information about the target set, and its variations can reflect the heterogeneity of the set.

From lab experiments, CT-images, or outcrop maps, many researchers collected 2-D mappings of fracture networks and performed the fractal and multifractal analysis (Barton, 1995; Berkowitz and Hadad, 1997; Cello, 1997). However, natural fractures are always three-dimensional rather than two-dimensional in the subsurface. The fractal and multifractal analyses on 3-D fracture networks are rarely conducted. The main difficulty is that detailed mappings of subsurface fracture networks are almost impossible with current approaches, including outcrop observations and seismic mappings. Furthermore, a comprehensive investigation of the fracture geometrical properties on the fractal and multifractal characteristics of complex 3-D fracture networks is largely insufficient, such as fracture orientations, lengths, positions of fracture centers, and system sizes. It is because obtaining systematic 3-D geological data with various fracture features is extremely difficult. Stochastic discrete fracture network (SDFN) modeling method provides a practical alternative. In 3-D SDFN, simple shapes represent fractures, such as polygons, disks, and ellipses. Fracture geometries, such as orientations, lengths, and center positions, are described with different statistic distributions (Lei et al., 2017). Although the geometry details of natural fractures are significantly simplified, the topological structures, like the intersection relationship, are well preserved. HatchFrac is an

efficient DFN modeling software (Zhu et al., 2021a), which makes it possible to generate systematic fracture networks and conduct statistic analysis. Zhu et al. (2022) used the stochastic discrete fracture network models to systematically investigate the impacts of fracture proprieties on the fractal and multifractal characteristics in complex 2-D fracture networks. In this work, we further extend their work to 3-D fracture networks. The impact of important geometrical properties, such as fracture lengths, center positions, and orientations, on the complexity characterization of 3-D stochastic fracture networks, are studied. Artificially generated fracture networks always have a finite size, and different system sizes are included to evaluate the finite-size effect.

We extend the conventional image-based box-counting technique (Barton, 1995) to calculate the fractal and multifractal descriptors of 3-D fracture networks. This research represents a 3-D fracture with a convex polygon for simplicity. Convex polygons have more degrees of freedom than a simple disk shape, and it is also convenient to change their shapes to elliptical shapes or other polygon shapes by minor adjustments to the number of vertices and coordinates. Furthermore, it is also easier to analyze intersection relationships in convex polygons (Zhu et al., 2021a). It is worthwhile to mention that the specific shape of fractures is insignificant when the number of fractures is large (Jing and Stephansson, 2007). Different statistical distributions are implemented to describe fracture geometries (Bonnet et al., 2001a). A power-law distribution is predominately adopted to describe fracture lengths because of extensive observations from outcrop maps and lab experiments (Bour and Davy, 1997; Bonnet et al., 2001b). The exponent of the power-law distribution, a, determines the probability of generating large fractures. If a is large, it will be difficult to generate large fractures. The von Mises—Fisher distribution can describe the orientation of fractures (Song et al., 2001; Whitaker and Engelder, 2005). A concentration parameter κ represents the concentration level of the fracture orientations. Uniform spatial density distribution (Bour and Davy, 1997) and fractal spatial density distribution (Darcel et al., 2003) are used to describe fracture center positions. A fractal spatial density distribution causes fracture

centers to cluster, which is commonly observed in reality(Akara et al., 2021). A fractal dimension, F_D, constrain the clustering degree. For 3-D fracture networks, if $F_D < 3.0$, there will be clustering effects, and the distribution reduces to a uniform spatial density distribution when $F_D = 3.0$. A smaller fractal dimension refers to more server clustering effects. Please note that the fractal dimension (F_D) is the key parameter in the fractal spatial density distribution, and it is completely different from the fractal dimension calculated in the fractal analysis.

This paper is organized as follows. In Section 2, techniques for constructing three-dimensional (3-D) stochastic fracture networks are introduced. The box-counting method to calculate fractal and multifractal descriptors is covered. In Section 3, impacts of different fracture geometrical properties on the complexity of 3-D fracture networks are presented. The input/output correlation method is adopted to analyze the sensitivity of fracture geometrical parameters on the fractal and multifractal patterns. Finally, important findings are concluded in Section 4.

2. Methods and materials

In this section, we introduce the process to implement the SDFN model and generate 3-D fracture networks. Detailed procedures to apply the box-counting method for calculating fractal and multifractal descriptors are presented.

2.1. Construction of three-dimensional stochastic discrete fracture networks

Accurate information of natural fracture networks in the subsurface is unavailable with current technologies. Fractures in the subsurface also have complex and irregular shapes. To reduce modeling complexity, four-vertex convex polygons are adopted to simulate fractures in 3-D. Each fracture is described by three key geometrical parameters, i.e., fracture orientations, sizes, and fracture center positions, characterized by different statistic distributions. Fracture lengths is widely described by a power-law distribution (Bour and Davy, 1997).

$$N(l) = \beta l^{-a}, \tag{1}$$

where $N(l)dl$ is the number of fractures with their lengths varying in the interval of l and $l + dl$, β is the proportionality coefficient. a is the exponent of the power-law distribution, which usually varies between 2.0 and 3.0 (Bonnet et al., 2001b; Zhu et al., 2018). To successfully generate length variables, a minimum and maximum length are required, which are set to be 1 and 100,000 units in this work. For 3-D fracture networks, fracture sizes are more appropriate than lengths to describe the fracture geometry. Therefore, we first generate convex polygons with a random side length varying between 0 and 1. Then a scaling operation is performed with l as the scaling factor to change the size of the 3-D fracture.

The von Mises–Fisher distribution (Whitaker and Engelder, 2005) is usually adopted to describe fracture orientations.

$$F(\vec{x}, \vec{\mu}, \kappa) = B(\kappa) \exp(\kappa \vec{\mu}^T \vec{x}), \tag{2}$$

where $B(\kappa)$ is the constant for normalization. $\vec{\mu}$ is the mean orientation. κ is a concentration parameter and refers to the degree of concentration with respect to $\vec{\mu}$. Here, $\vec{\mu}$ is set as $[1, 0, 0]$ and κ varies between the interval of [0, 20].

Fracture center positions are described with a fractal spatial density distribution (Darcel et al., 2003). A fractal dimension F_D is used to generate the fractal spatial density distribution. However, F_D is totally different from the fractal dimension of the complete fracture network. F_D varies between 2.0 and 3.0 for 3-D space. When $F_D < 3.0$, fracture centers are clustered, and the clustering degree increases with decreasing F_D.

The 3-D discrete fracture networks are generated by in-house DFN modeling software, HatchFrac. Detailed information on the cluster-check algorithm can be found at Zhu et al. (2021a). In 2-D fracture networks, the termination criterion of generating new fractures is forming a spanning cluster (Zhu et al., 2022) because fracture networks observed from outcrop maps usually show good connectivity, and connected fracture networks are essential for fluid transportation in formations with low permeability. However, real fracture networks are always three-dimensional instead of two-dimensional. 2-D fracture networks can only

be regarded as cross-section maps of the corresponding 3-D fracture networks. If the cross-section map has a spanning cluster formed, the corresponding 3-D fracture network should have a much higher intensity than the intensity at percolation (Zhu et al., 2021c). The percolation status here refers to the state where a spanning cluster is formed. A spanning cluster is a cluster of connected fractures, shown as red fractures in Fig. 1. It connects six faces of the 3-D domain, and serves as the main fluid flow pathway in subsurface formations with low permeability. Therefore, we consider two stages of the 3-D fracture network in this research. Stage one is a percolative stage when a spanning cluster is formed in the 3-D fracture system, but 2-D fracture networks from the cross-section maps are usually sparse and poorly connected. Stage two is an over-percolative stage when a spanning cluster is formed in the 2-D cross-section map of the 3-D fracture network, and the corresponding 3-D fracture network has an intensity much higher than the intensity at stage one. Without loss of generality, the cross-section map is taken from the middle-position of the 3-D fracture networks as shown in Fig. 1(b), which usually have an intermediate fracture intensity. Fig. 1 presents a demonstration of the two stages. The spanning cluster is marked red, while fractures disconnected to the spanning cluster are marked green. Both stages are possible in reality, and they have a spanning cluster formed, which is essential for the fluid flow in the subsurface. Stage two might be more common since many outcrop maps collected have formed a spanning cluster (Zhu et al., 2021c). However, the outcrop maps collected are usually biased because regions with well-developed fractures are preferred.

2.2. Fractal and multifractal descriptors

The fractal dimension measures the spatial coverage of the examined set. A larger fractal dimension indicates a higher spatial coverage. The box-counting method is a convenient and robust method to calculate the fractal dimension of any examined set. Boxes with varying sizes (r), are superimposed on a fracture network, as shown in Fig. 2. Under each box size, the number of boxes containing fractures is recorded, denoted as N_r. If the examined set shows a

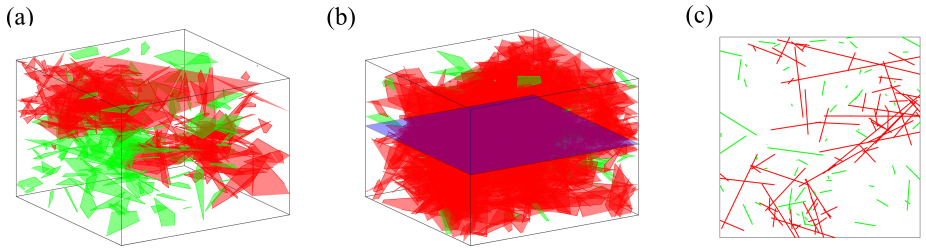

Figure 1: (a) A 3-D fracture network at stage one; (b) A 3-D fracture network at stage two; (c) The cross-section map of the 3-D fracture network at stage two (b) and the cross-sectional plane is marked blue in (b). The red polygons in (a) and (b) and red line segments in (c) compose the spanning cluster. The green polygons in (a) and (b) and green line segments in (c) refer to locally connected clusters. For 3-D fracture networks, the fracture lengths obey a power-law distribution with a = 3, and an uniform distribution describes orientations. The positions of fracture centers follow a fractal spatial density distribution with $F_D = 2.5$.

fractal pattern, N_r and r, the following relation should hold:

$$N_r = r^{-D}, \tag{3}$$

where D is the fractal dimension of the examined set, obtained from the slope of a linear fitting of $\ln(N_r)$ and $\ln(1/r)$. For 3-D fracture networks, the fractal dimension varies between 2.0 and 3.0, where 3.0 is the euclidean dimension of a 3-D volume.

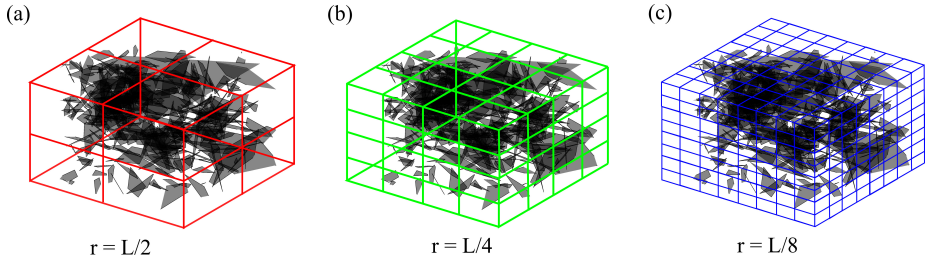

Figure 2: Demonstration of the box-counting method to calculate the fractal and multifractal descriptors of a 3-D fracture network

Moreover, the multifractal spectrum reveals more information of an examined set, such as the heterogeneity. We detail the corresponding step-by-step procedure as follows:

1. A probability distribution function is defined for a 3-D fracture network:

$$p_i(r) = \frac{A_i}{\sum_{i=1}^{N} A_i}, \tag{4}$$

where A_i is the total area of all fracture segments included in the i^{the} box, r is the box size, N is the number of boxes.

2. A partition function (Halsey et al., 1986) is calculated, which is the summation of q^{th} power of Eq. 4:

$$\chi_q(r) = \sum p_i(r)^q, \tag{5}$$

where q is the order of the probability moment, ranging from $-\infty$ to $+\infty$ for a complete spectrum. Different q can magnify the significance of different boxes with different values of p_i. The negative and positive values of q can emphasize the significance of boxes with small and large p_i, respectively. It is impossible to have infinite values of q, and usually, an interval of $[-18, 18]$ is sufficient for the implementation. If the examined set has multifractal features, the linear relation below should hold:

$$\chi_q(r) \propto r^{\tau(q)}, \tag{6}$$

where $\tau(q)$ is a mass exponent. Its value is obtained by a linear fitting of $\ln(\chi_q(r))$ and $\ln(r)$ since:

$$\tau(q) \propto \frac{\ln(\chi_q(r))}{\ln(r)}, \tag{7}$$

3. Legendre transform is implemented on $\tau(q)$, which yields the multifractal spectrum $f(\alpha)$

$$\alpha = \frac{d\tau(q)}{dq} \propto \frac{\sum_{i=1}^{N} p_i(r)^q \ln(p_i(r))}{\sum_{i=1}^{N} p_i(r)^q \ln(r)}, \tag{8}$$

$$f(\alpha) = \alpha q - \tau(q), \tag{9}$$

where α is the Lipschitz-Hölder exponent. Different α values indicate singular degrees of different fractal subsets. $f(\alpha)$ is corresponding fractal dimension of the subset characterized by α.

Salat et al. (2017) suggested an average over several samples to avoid the accuracy decrease caused by the numerical Legendre transform. Therefore, all results discussed below are averaged over ten independent realizations.

2.3. Sensitivity analysis

The fractal dimension and multifractal spectrum can characterize different aspects of fracture networks' complexity. In this work, we analyze three fracture geometrical properties, including fracture orientations, lengths, and fracture center positions, and one property of the fracture system, the system size. The system size is different from the other geometrical properties because it describes the complete system instead of individual fracture. However, the system size can still impact the configuration of a fracture network.

We consider 10 levels for each geometrical parameters (a, F_D, κ) in different intervals. Three levels of the system sizes are considered ($\{10,\ 20,\ 30\}$). Considering the computational capacity, the maximum system size is set as 30. A full factorial design of these four parameters needs 3,000 cases, and each case should be stabilized by averaging over ten realizations. Therefore, a huge amount of computational resources are required. To reduce computation resources, we generate 100 orthogonal cases concerning a, F_D, and κ for a given system size (Karna et al., 2012). The responses of the sensitivity analysis are the single fractal dimension (D) and the difference of the singularity exponent ($\Delta\alpha$). Abundant information is available from a multifractal spectrum, such as different values of α, their corresponding fractal dimension $f(\alpha)$, and generalized dimension D_q. However, the difference of the singularity exponent ($\Delta\alpha$) is better to describe the heterogeneity of the set since α is an indicator of the singular degree of fractal subsets. Therefore, $\Delta\alpha$ is chosen to represent the multifractal spectrum and serves as a response in the sensitivity analysis. The detailed information of the parameters considered for the sensitivity analysis is summarized in Table. 1.

In this paper, we assume the geometrical parameters of fracture networks are independent of each other. To quantify the impact of each geometrical parame-

Table 1: Summary of parameters for the sensitivity analysis

Parameter	Range/Type	Usage / Definition
a (power-law distribution)	[2, 3]/Input	Describing fracture lengths
F_D (fractal spatial density distribution)	[2, 3]/Input	Describing fracture center positions
κ (von Mises–Fisher distribution)	[0, 20]/Input	Describing fracture orientations
L (system size)	{10, 20, 30}/Input	Describing system sizes
D	Response	Single fractal dimension
$\Delta\alpha$	Response	Difference of the singularity exponent α

ter on the fractal and multifractal characteristics (D and $\Delta\alpha$), an input/output correlation method is adopted because it is simple, robust and straightforward for independent input parameters. To determine the sensitivity of the response R with respect to the input parameters $\vec{X}$, the correlation coefficient of each pair of R and X_i is calculated. For the i^{th} parameter, suppose that X_i has n samples, $X_i = \{X_i^{(1)}, X_i^{(2)}, X_i^{(3)}, \ldots, X_i^{(n)}\}$, and the corresponding response R also have n elements, $R = \{R^{(1)}, R^{(2)}, R^{(3)}, \ldots, R^{(N)}\}$. The correlation coefficient of X_i and R is calculated by:

$$\rho_i = \rho(X_i, R) = \frac{E[(X_i - \mu_i)(R - \mu_R)]}{\sigma_i \sigma_R}, \tag{10}$$

where μ_i and σ_i are the expected value and standard deviation of X_i, μ_R and σ_R are the corresponding values of R. the magnitude of the correlation coefficient reveals the significance of each factor on the response. The input vector included a, F_D, κ and L, for 3-D fracture networks. The response parameter is the fractal dimension (D) and the difference of the singularity exponent ($\Delta\alpha$).

3. Results and discussion

Considering the computational cost, six values are chosen for the box sizes in the box-counting method:

$$b_s = \frac{L}{2^i} = Lr, \qquad i = 0, 1, 2, 3, 4, 5 \tag{11}$$

where b_s is the box size, r is the dimensionless box size with respect to the system size, L.

From a linear fitting of $\ln(N(r))$ and $\ln(1/r)$, the fractal dimension is obtained. At the initial state, when only one box is superimposed on the fracture network, the box size is L, and the corresponding number of boxes is one. The fitting curve must pass a fixed point (0, 0) in the linear fitting. This constraint is significant for the fractal dimension calculation but ignored by many researchers. Fig. 3 shows the fractal dimensions calculated for fracture networks at both stages (Fig. 1(a,b)). The fracture network at stage one has a smaller fractal dimension (2.70) than the fracture network at stage two (2.90).

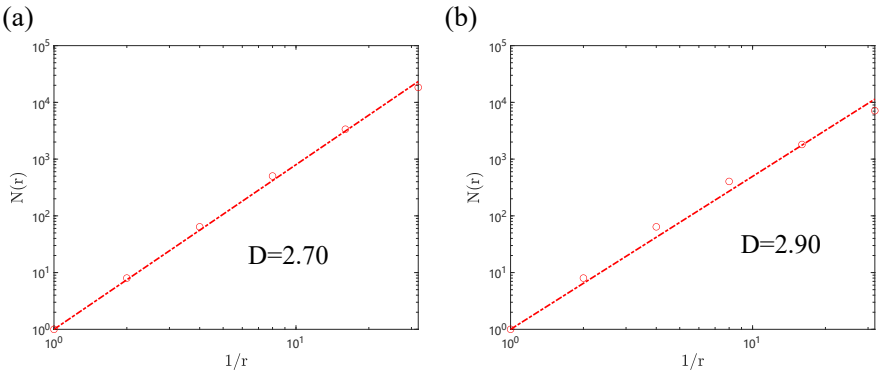

Figure 3: The calculated fractal dimension D for fracture networks in Fig. 1 (Left:Fig. 1a ; Right: Fig. 1b). The red dash line is the linear fitting result.

To perform multifractal analysis, we should test the linear relationship between $\ln(\chi_q(R))$ and $\ln(r)$. The constraint of passing (0,0) should be satisfied. Fig. 4 (a) shows the double-log plot of $\chi_q(r)$ and r of the fracture network in Fig. 1(a). If the fracture network has multifractal features, a linear relation between $\ln(\chi_q(R))$ and $\ln(r)$ should hold. In Fig. 4(b), the correlation coefficients of these two parameters for different q values are shown. The correlation coefficient are either 1 or -1, supporting the linear relation. Variations of the correlation coefficient happen with $q = 1$ because the corresponding $\chi_q(r) = 1$ for all box sizes. $\ln(\chi_q(R))$ and $\ln(r)$ fall on a horizontal line and cause vibrations of the correlation coefficient as shown in Fig. 4(b) . If $q = 0$, the corresponding

$\chi_q(r) = N(r)$, where the fitting slope yields $-D$. The multifractal spectrum of the considered fracture network in Fig. 1 (a) are presented in Fig. 4 (c). For fractal subsets with the same α value, they have a unique fractal dimension $f(\alpha)$. Fig. 5 shows results of the fracture network at stage 2 (Fig. 1(b)). $\ln(\chi_q(r))$ and $\ln(r)$ show a good linear relationship and the multifractal spectrum is provided. The value of α suggests the singular degree of fractal subsets. However, the difference of α, $\Delta\alpha$, can characterize the heterogeneity of the complete fracture system. For two fracture networks shown in Fig. 1(a, b), $\Delta\alpha$ equal 5.81 and 5.88, respectively.

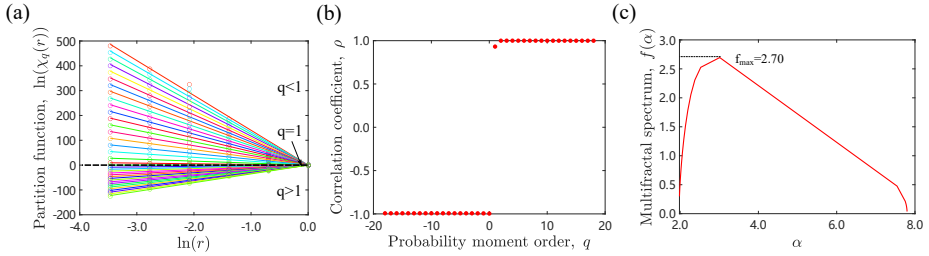

Figure 4: Stage 1: (a) Double-Log plot of $\chi_q(r)$ and r. Scatter points and their linear fitting under the same q value are shown in the same color. (b) Correlation coefficient of each linear fit in (a), (c) The multifractal spectrum of Fig. 1 (a)

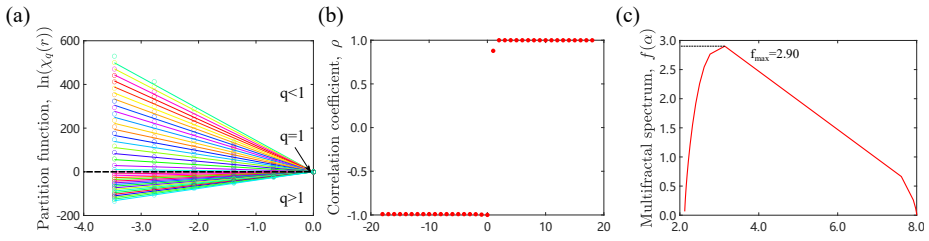

Figure 5: Stage 2: (a) Doule-Log plot of $\chi_q(r)$ and r. Scatter points and their linear fitting under the same q value are shown in the same color. (b) Correlation coefficient of each linear fit in (a). (c) The multifractal spectrum of Fig. 1 (b)

The next two sections present the results of D and $\Delta\alpha$ of the fracture networks with different configurations. Impacts of each geometrical property on the fractal and multifractal characteristics are also analyzed. The results of

Table 2: Summary of statistics of D and $\Delta\alpha$

Response	D (stage one)	D (stage two)	$\Delta\alpha$ (stage one)	$\Delta\alpha$ (stage two)
Number of scenarios	300	300	300	300
Max	2.96	2.99	6.58	6.06
Min	2.57	2.85	4.92	2.50
Mean	2.78	2.96	5.67	5.00
Median	2.79	2.97	5.67	5.11
Standard deviation	0.08	0.03	0.27	0.56
P_{10}	2.64	2.90	5.33	4.32
P_{50}	2.78	2.97	5.67	5.11
P_{90}	2.87	2.99	6.01	5.56

fracture networks in two stages are presented simultaneously.

3.1. Behavior of D in 3-D fracture networks at two stages

In this section, we present the behavior of the single fractal dimension, D, in complex 3-D fracture networks at both stages. The sensitivity of each geometrical parameter on D is analyzed. The mean values of the single fractal dimension (D) over ten realizations at both stages are shown in Figs. 6(a) and (b). The cumulative plots of D at both stages are show in Figs. 6(c) and (d), where estimates of P_{10}, P_{50} and P_{90} are denoted. For stage one, D scatters in the interval between 2.50 and 2.95. The P_{10}, P_{50} and P_{90} estimates are 2.65, 2.77 and 2.87, respectively. For stage two, D varies between 2.84 and 3.0, and the estimates are 2.90, 2.97, and 2.99, respectively. D at stage two has a narrower range but a much higher value than results at stage one. A larger fractal dimension refers to better space coverage. Therefore, fracture networks at stage two have better coverage of 3-D space than fracture networks at stage one, mainly because of the large fracture intensity at stage two. From Zhu et al. (2021c)'s observations, the fracture intensity at stage two can be more than 3.5 times of the intensity at stage one. A detailed summary of the statistics of D and $\Delta\alpha$ over 300 cases at both stages is presented in Table. 2.

Different colors in Fig. 6 refer to calculated D in fracture networks with

varying system sizes. It is not straightforward to observe the difference caused by different system sizes from the scatter plots. Therefore, the mean value of D over 100 cases under different sizes are calculated and shown as different line segments. It turns out that fracture networks with a larger system size have a larger mean value of D. The system size is a property of the system instead of a geometrical property of fractures. However, different system sizes can still change the configuration of a fracture network. It should be noted that the system sizes and scales are completely different because all fracture geometric properties honor the same statistic distributions regardless of system sizes. For fracture lengths, the intervals of sampling become wider for a larger fracture system, but the resolution is fixed with the same minimum fracture length l_{min}. As the system size increases, the population of fractures generally increases because more samples of fracture orientations, lengths, and center positions are collected, forming a more complex fracture network.

Generated fracture networks always have a finite size and variations of a statistic parameter in a finite fracture network may depend on the system size. To evaluate the finite-size effect of D and $\Delta\alpha$, we further extend the Eq. 12 adopted by Bour and Davy (1997) for percolation parameters.

$$f(L) - f^{\infty} \sim \Delta f(L), \tag{12}$$

where L is the system size, $f(L)$ and f^{∞} are the quantities examined in a system with a finite and infinite size, respectively. $\Delta f(L)$ is the standard deviation of $f(L)$.

Standard deviations of D over ten realizations are shown in Fig. 7. The standard deviation of D varies between 0 and 0.18. Mean values of the standard deviations in fracture networks with different system sizes are denoted for better visualization. The mean values of the standard deviation slightly decrease with the increasing system sizes, indicating a weak finite-size effect. Therefore, a large fracture system is more suitable for a stable fractal dimension estimation.

Fractal dimension measures the system complexity regarding spatial coverage. However, the sensitivity of geometrical parameters on the fractal dimension

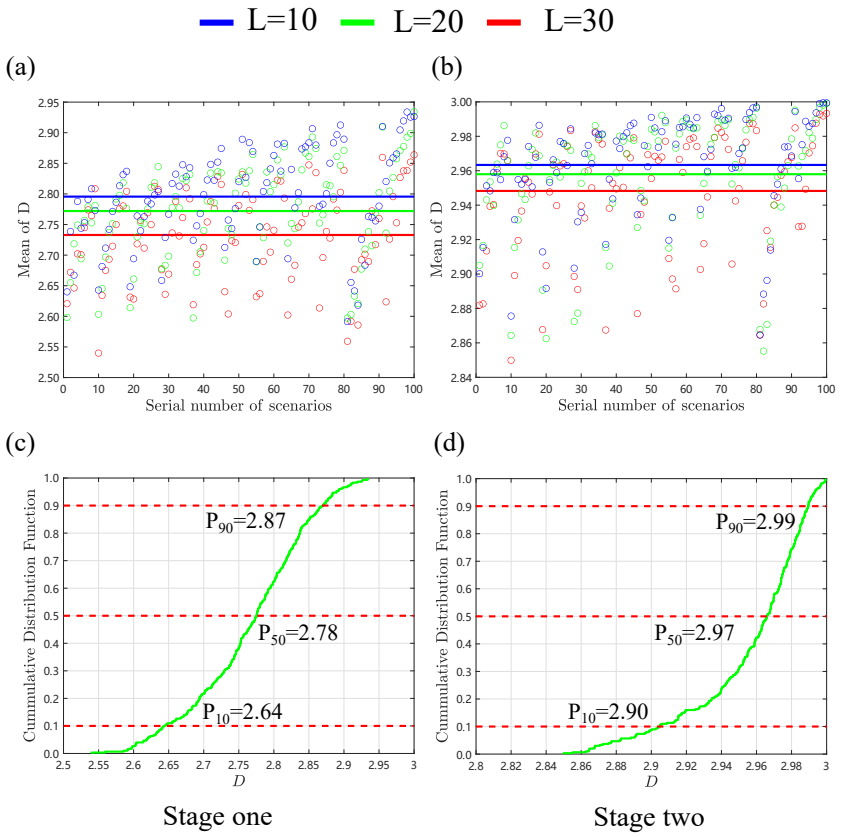

Figure 6: (a, b) Scatter plots of means of the single fractal dimension, D, over 10 realizations at two stages. Different colors represent results under different system sizes. The line segments are the corresponding mean values of the scatter points. (c, d) the CDF of D at two stages

of the fracture network is rarely investigated. With the input/output correlation method, the impacts of geometrical properties of fractures, including the fracture length (a), positions of fracture centers (F_D) and fracture orientations (κ), and the system size are presented. The results of the sensitivity analysis of each parameter on D are shown in Fig. 8

At stage one, a, L, and κ have a positive correlation with D, meaning that a large fracture network dominated by small fractures with concentrated orientations tend to have a large fractal dimension and cover more space. F_D has a slightly positive correlation with D, indicating that the single fractal dimension

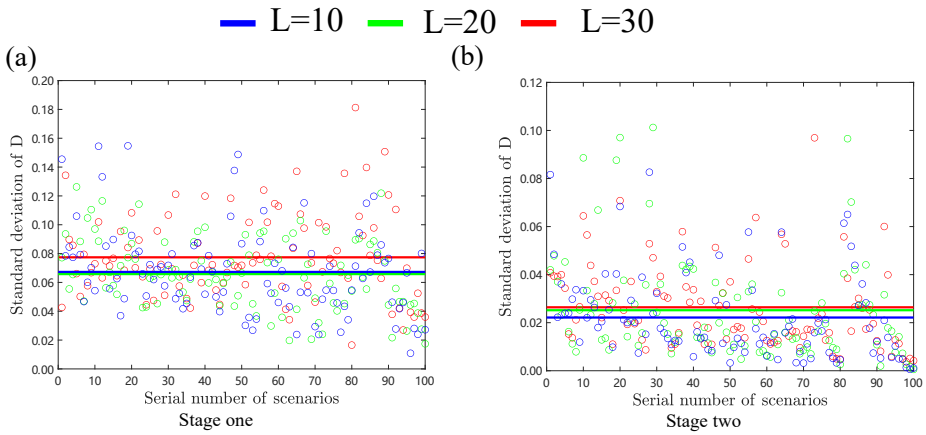

Figure 7: Scatter plots of standard deviations of the single fractal dimension, D, over ten realizations at two stages. Different colors represent results under different system sizes. The line segments are the corresponding mean values of the scatter points.

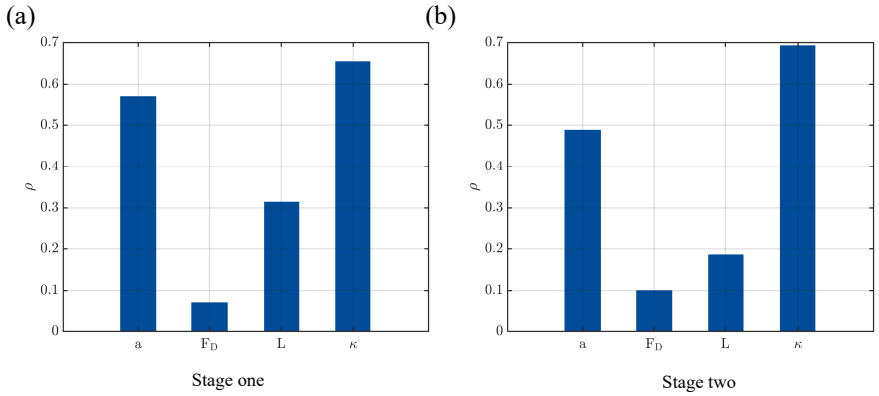

Figure 8: The sensitivity analysis of each factor on the fractal dimension (D) at two stages

is insensitive to clustering effects. Similar observations are found in 2-D fracture networks (Zhu et al., 2022).

At stage two, the sensitivity of each property does not change much. The orientation concentration parameter κ has the most significant impact on D, following the exponent a and the system size L. The clustering effect is weakly correlated with D. Clustering effects represent the heterogeneity of the fracture network. Therefore, a fractal dimension cannot capture heterogeneity.

3.2. Behavior of $\Delta\alpha$ in 3-D fracture networks at two stages

In this section, we present the behavior of the difference of the singularity exponent, $\Delta\alpha$, in complex 3-D fracture networks at both stages. The sensitivity of each geometrical parameter on $\Delta\alpha$ is analyzed.

The mean values of $\Delta\alpha$ over ten realizations at both stages are shown in Figs. 9(a, b). The cumulative plots of $\Delta\alpha$ at both stages are show in Fig. 9(c, d), where estimates of P_{10}, P_{50} and P_{90} are denoted. For stage one, $\Delta\alpha$ scatters in the interval between 4.8 and 6.6. The P_{10}, P_{50} and P_{90} estimates are 5.33, 5.67 and 6.01 respectively. For stage two, $\Delta\alpha$ varies between 2.0 and 6.5. The corresponding estimates are 4.32, 5.11, and 5.56, which have a much wider range and relatively lower values than the results at stage one. A larger $\Delta\alpha$ value indicates a higher heterogeneity degree. Fracture networks at stage two have a much higher fracture intensity than stage one. Therefore, more fractures tend to cover more void space in the system and make the fracture system less heterogeneous.

Different colors refer to results in fracture networks with varying system sizes. The mean value of $\Delta\alpha$ over 100 cases under different sizes are calculated and shown as different line segments in Figs. 9(a, b). At stage one, fracture networks with a larger system size have a larger mean value of $\Delta\alpha$. However, the variations of $\Delta\alpha$ at stage two in fracture networks with different system sizes are small, and fracture networks with a larger system size even have a slightly smaller $\Delta\alpha$ value. Therefore, the heterogeneity of a fracture network at stage two does not increase with increasing system sizes.

The standard deviations of $\Delta\alpha$ over ten realizations are shown in Fig. 10. Mean values of the standard deviations in fracture networks with different system sizes are denoted with varying line segments for better visualization. For stage one, $\Delta\alpha$ has standard deviations ranging between 0.2 and 1.2. Mean values of the standard deviations for different system sizes are almost the same. For stage two, standard deviations of $\Delta\alpha$ vary between 0.2 and 1.0, and slightly increase with increasing system sizes. Therefore, there are no finite-size effects on $\Delta\alpha$. It is unnecessary to have a large system to obtain the stable $\Delta\alpha$ results

for a fracture network with predesigned configurations.

Impacts of the geometrical properties of fractures, including the fracture length (a), positions of fracture centers (F_D) and fracture orientations (κ), and the system size, on $\Delta\alpha$ are presented in Fig. 11.

At stage one, the fracture length (a) and system sizes (L) positively correlate with $\Delta\alpha$, indicating that a large system dominated by small fractures is more likely to have a larger $\Delta\alpha$ and more heterogeneous. The clustering effect represented by F_D has a significant negative correlation with $\Delta\alpha$, which means the clustering effect can make the fracture system more heterogeneous, and $\Delta\alpha$ can capture the difference caused by clustered center positions. The concentration of fracture orientations has a slightly negative correlation, indicating an insignificant impact on $\Delta\alpha$. We test the correlation coefficient between the F_D and $\Delta\alpha$ with different system sizes, and we find that coefficient decreases with increasing system sizes. For fracture networks with system sizes of 10, 20, and 30, the correlation coefficients between F_D and $\Delta\alpha$ are -0.40, -0.55, -0.62. In larger fracture networks, the impact of clustering effects on the $\Delta\alpha$ is more significant. In a small fracture system, 3-D fractures can interact with all the other fractures in a volume, while 2-D fractures can only intersect fractures in the same plane. Therefore, 2-D fracture networks are more sensitive to the local clustering effects than 3-D fracture networks (Zhu et al., 2021b). However, the clustering effect can also be significant in 3-D fracture networks if the fracture networks are large enough with abundant fractures.

At stage two, For $\Delta\alpha$, the sensitivity results significantly differ from stage one. Instead of positive correlations, the exponent a and system size negatively correlate with $\Delta\alpha$. The clustering effect (F_D) has the most significant impact on $\Delta\alpha$, following the orientation concentration κ. Therefore, in a fracture network with pervasive fractures, small fractures, and a large system size can reduce the heterogeneity. The clustering effect and concentrated orientations can enhance the heterogeneity.

The correlation of D and $\Delta\alpha$ at two stages are shown in Fig. 12. At stage one, the correlation is 0.08, indicating that the D and $\Delta\alpha$ are almost independent

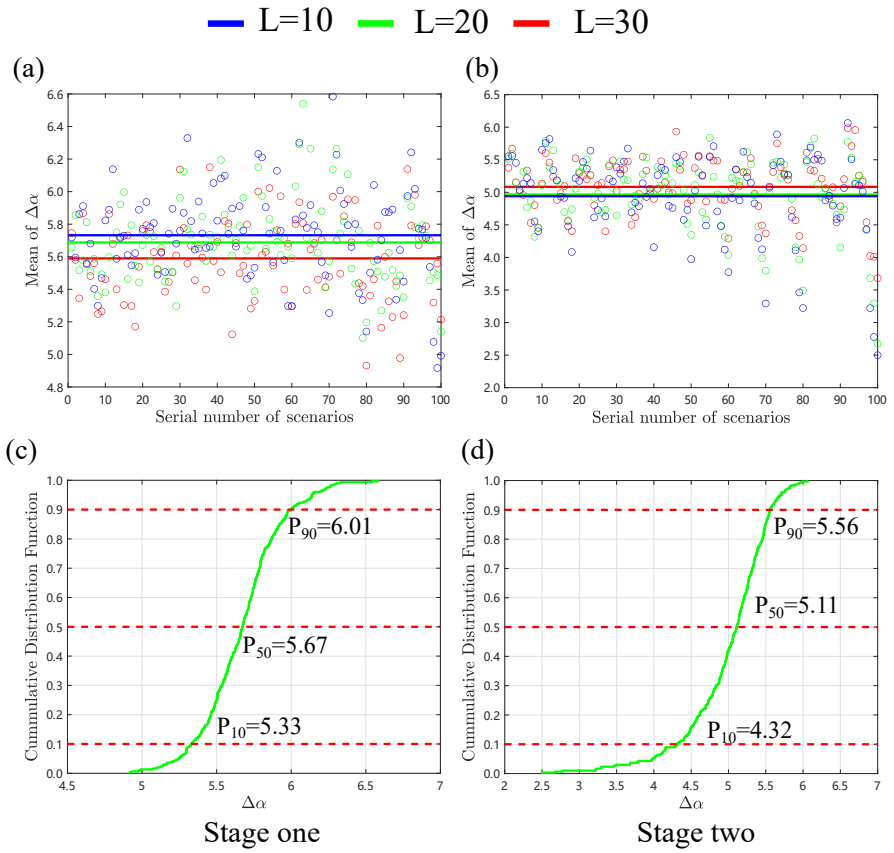

Figure 9: (a, b) Scatter plots of the mean values of the difference of the singularity exponent, $\Delta\alpha$, over 10 realizations at two stages. Different colors represent results under different system sizes. The line segments are the corresponding mean values of the scatter points. (c, d) the CDF of $\Delta\alpha$ at two stages

of each other. For stochastic discrete fracture networks in 2-D, D and $\Delta\alpha$ are positively correlated(Zhu et al., 2022). However, for 3-D fracture networks, these two parameters have different behaviors and are uncorrelated. At stage two, the correlation is -0.58. However, the negative correlation is significant when the fractal dimension D is close to 3.0, meaning the fracture network will cover the full 3-D space. In this condition, the heterogeneity degree becomes insignificant and causes $\Delta\alpha$ to decrease. In Zhu et al. (2022)'s work, they collected 80 outcrop maps and calculated their fractal dimension and multifractal spectrum. In real

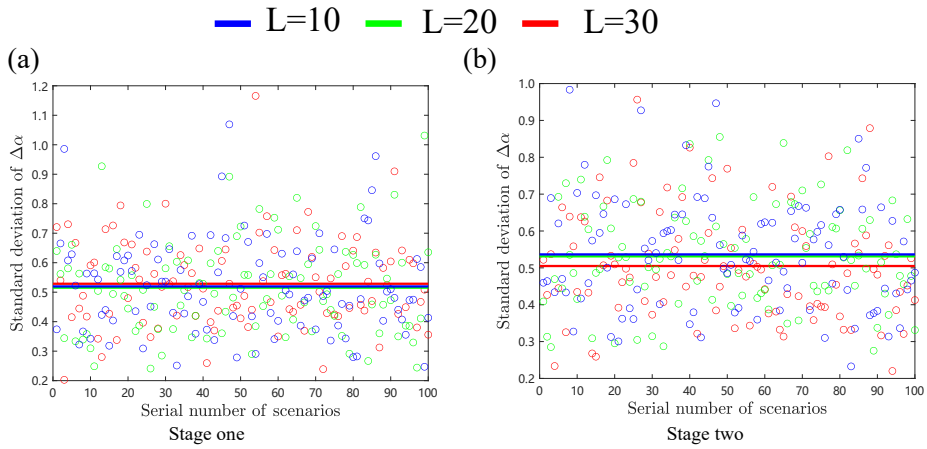

Figure 10: Scatter plots of the standard deviations of the difference of the difference of the singularity exponent, $\Delta\alpha$, over 10 realizations. Different colors represent results under different system sizes. The line segments are the corresponding mean values of the scatter points.

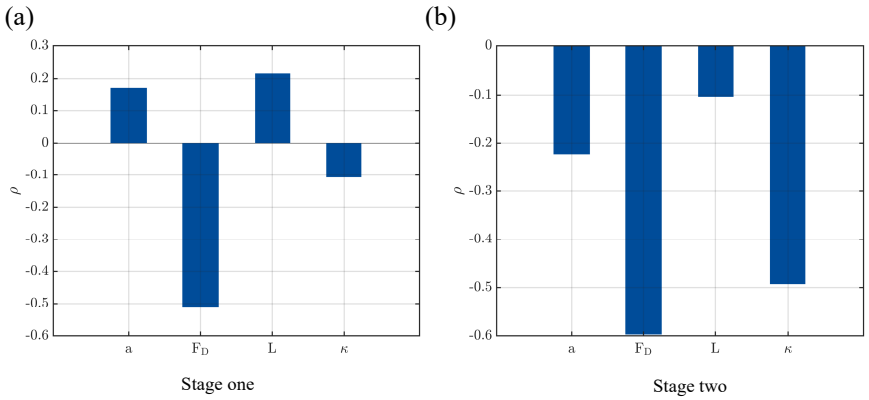

Figure 11: The sensitivity analysis of each factor on the difference of the singularity exponent, $\Delta\alpha$, at two stages

outcrop maps, they find a slightly negative correlation between D and $\Delta\alpha$, which is closer to the results of 3-D fracture networks at stage two. In general, the fractal dimension and multifractal spectrum can be regarded as independent measures of different aspects of fracture systems. One characterizes the spatial coverage, and the other one measures the heterogeneity.

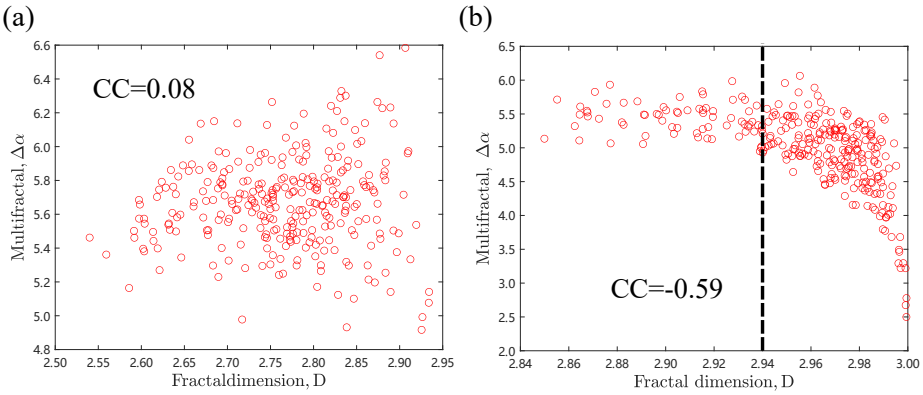

Figure 12: Correlations between D and $\Delta\alpha$ at two stages (Left: stage one; Right: stage two)

For 2-D fracture networks, we can calculate the fractal dimension and multifractal spectrum of outcrop maps and compare the results of discrete fracture networks and real fracture networks. However, it is extremely difficult to have detailed information of real 3-D fracture networks in the subsurface with current technologies. Therefore, it is also impractical to check the fractal and multifractal features of natural 3-D fracture networks. Stochastic discrete fracture networks are far different from real fracture networks. However, they still share similarities in their geometrical properties and topological structures. Therefore, stochastic discrete fracture networks can be a practical alternative to mimic subsurface fracture networks. More importantly, we can systematically analyze the impacts of fracture geometries on fracture complexity. The quantitative values of fractal dimensions and multifractal spectrum might not be important, but the qualitative observations of the variations of D and Δ can provide valuable hints for a better understanding of the subsurface structures. The complexity of fracture networks can be important to the geometrical and hydrological connectivity of fracture networks. However, this work focuses more on the fractal and multifractal characteristics of 3-D stochastic discrete fracture networks and the impacts of fracture geometries on those characteristics. The correlations and impacts between fracture complexity and connectivity can be investigated in future research.

4. Conclusions

This work implements the stochastic discrete fracture network model methods to systematically investigate the fractal and multifractal characteristics of complex 3-D fracture networks at two stages. Different geometrical properties are considered, such as fracture orientations, lengths, and center positions. Their impacts on the fractal and multifractal characteristics are evaluated. The finite-size effects and the impact of system sizes on the responses are included. Key conclusions are summarized below.

- For stage one, where a spanning cluster is formed in the 3-D fracture network, the power-law exponent (a) and the system size (L) and the concentration parameter of fracture orientations (κ) have a positive correlation with D. κ is the most significant factor on D among the three parameters. The clustering effect F_D has a weak correlation with D, indicating that D is insensitive to clustering effects.

  However, for $\Delta\alpha$ in stage one, F_D has a significant negative correlation, indicating that multifractal spectrum are sensitive to clustering effects. κ has a slightly negative correlation with $\Delta\alpha$, while a and L have a weak positive correlation.

- For stage two, where a spanning cluster is formed in the cross-section map of a 3-D fracture network, the results of sensitivity of each geometrical parameter and the system sizes on D are the same as the results in stage one. κ is the most significant parameter, following a and L. F_D has a weak correlation with D.

  However, for $\Delta\alpha$ at stage two, the sensitivity results are different from results at stage one concerning a and L, and they have negative instead of positive correlations. Impacts of κ and F_D become more significant. $\Delta\alpha$ is a good indicator for the heterogeneity of fracture networks.

Data Availability

All data are synthetically generated by our in-house built DFN modeling software, HatchFrac. The C++ code for generating 2-D and 3-D fracture networks are available online (https://data.mendeley.com/datasets/zhs97tsdry/1)

Declaration of Competing Interest

The authors declare that they have no known competing financial interests or personal relationships that could have appeared to influence the work reported in this paper.

Acknowledgments

This project was supported by the National Key Research and Development Program of China (No. 2019YFA0708704). The authors would like to thank all editors and anonymous reviewers for their comments and suggestions.

References

Akara, M.E.M., Reeves, D.M., Parashar, R., 2021. Impact of horizontal spatial clustering in two-dimensional fracture networks on solute transport. J. Hydrol. 603, 127055.

Aviles, C., Scholz, C., Boatwright, J., 1987. Fractal analysis applied to characteristic segments of the San Andreas fault. J. Geophys. Res.: Solid Earth 92, 331–344.

Barton, C.C., 1995. Fractal analysis of scaling and spatial clustering of fractures, in: Fractals in the earth sciences. Springer, pp. 141–178.

Berkowitz, B., 2002. Characterizing flow and transport in fractured geological media: A review. Adv. Water Resour. 25, 861–884.

Berkowitz, B., Hadad, A., 1997. Fractal and multifractal measures of natural and synthetic fracture networks. J. Geophys. Res.: Solid Earth 102, 12205–12218.

Bonnet, E., Bour, O., Odling, N.E., Davy, P., Main, I., Cowie, P., Berkowitz, B., 2001a. Scaling of fracture systems in geological media. Rev. Geophys. 39, 347–383.

Bonnet, E., Bour, O., Odling, N.E., Davy, P., Main, I., Cowie, P., Berkowitz, B., 2001b. Scaling of fracture systems in geological media. Rev. Geophys. 39, 347–383.

Bour, O., Davy, P., 1997. Connectivity of random fault networks following a power law fault length distribution. Water Resour. Res. 33, 1567–1583.

Cello, G., 1997. Fractal analysis of a Quaternary fault array in the central Apennines, Italy. J. Struct. Geol. 19, 945–953.

Darcel, C., Bour, O., Davy, P., De Dreuzy, J., 2003. Connectivity properties of two-dimensional fracture networks with stochastic fractal correlation. Water Resour. Res. 39.

Dershowitz, W.S., Herda, H.H., et al., 1992. Interpretation of fracture spacing and intensity, in: The 33th us symposium on rock mechanics (USRMS), American Rock Mechanics Association.

Follin, S., Hartley, L., Rhén, I., Jackson, P., Joyce, S., Roberts, D., Swift, B., 2014. A methodology to constrain the parameters of a hydrogeological discrete fracture network model for sparsely fractured crystalline rock, exemplified by data from the proposed high-level nuclear waste repository site at Forsmark, Sweden. Hydrogeol. J. 22, 313–331.

Halsey, T.C., Jensen, M.H., Kadanoff, L.P., Procaccia, I., Shraiman, B.I., 1986. Fractal measures and their singularities: The characterization of strange sets. Phys. Rev. A 33, 1141.

He, X., Sinan, M., Kwak, H., Hoteit, H., 2021. A corrected cubic law for single-phase laminar flow through rough-walled fractures. Adv. Water Resour. , 103984.

Jing, L., Stephansson, O., 2007. The Basics of Fracture System Characterization–Field Mapping and Stochastic Simulations, in: Dev. Geotech. Eng.. Elsevier. volume 85, pp. 147–177.

Karna, S.K., Sahai, R., et al., 2012. An overview on taguchi method. Int. J. Eng. Math. Sci. 1, 1–7.

Lei, Q., Latham, J.P., Tsang, C.F., 2017. The use of discrete fracture networks for modelling coupled geomechanical and hydrological behaviour of fractured rocks. Comput. Geotech. 85, 151–176.

Mandelbrot, B.B., 1977. Fractals: form, chance, and dimension. volume 706. WH Freeman San Francisco.

Mandelbrot, B.B., 1982. The fractal geometry of nature. volume 1. WH freeman New York.

Matsumoto, N., Yomogida, K., Honda, S., 1992. Fractal analysis of fault systems in japan and the philippines. Geophys. Res. Lett. 19, 357–360.

Okubo, P.G., Aki, K., 1987. Fractal geometry in the san andreas fault system. J. Geophys. Res.: Solid Earth 92, 345–355.

Otsuki, K., Dilov, T., 2005. Evolution of hierarchical self-similar geometry of experimental fault zones: Implications for seismic nucleation and earthquake size. J. Geophys. Res.: Solid Earth 110.

Pérez-Flores, P., Veloso, E., Cembrano, J., Sánchez-Alfaro, P., Lizama, M., Arancibia, G., 2017. Fracture network, fluid pathways and paleostress at the tolhuaca geothermal field. J. Struct. Geol. 96, 134–148.

Prabhakaran, R., Bertotti, G., Urai, J., Smeulders, D., 2021. Investigating spatial heterogeneity within fracture networks using hierarchical clustering and graph distance metrics. Solid Earth 12, 2159–2209.

Priest, S.D., Hudson, J., 1976. Discontinuity spacings in rock, in: International Journal of Rock Mechanics and Mining Sciences & Geomechanics Abstracts, Elsevier. pp. 135–148.

Salat, H., Murcio, R., Arcaute, E., 2017. Multifractal methodology. Physica A 473, 467–487.

Shi, X., Pan, J., Hou, Q., Jin, Y., Wang, Z., Niu, Q., Li, M., 2018. Micrometer-scale fractures in coal related to coal rank based on micro-ct scanning and fractal theory. Fuel 212, 162–172.

Song, J.J., Lee, C.I., Seto, M., 2001. Stability analysis of rock blocks around a tunnel using a statistical joint modeling technique. Tunnelling Underground Space Technol. 16, 341–351.

Whitaker, A.E., Engelder, T., 2005. Characterizing stress fields in the upper crust using joint orientation distributions. J. Struct. Geol. 27, 1778–1787.

Wu, H., Zhou, Y., Yao, Y., Wu, K., 2019. Imaged based fractal characterization of micro-fracture structure in coal. Fuel 239, 53–62.

Zhu, W., Khirevich, S., Patzek, T., 2018. Percolation properties of stochastic fracture networks in 2d and outcrop fracture maps, in: 80th EAGE Conference and Exhibition 2018, European Association of Geoscientists & Engineers. pp. 1–5.

Zhu, W., Khirevich, S., Patzek, T.W., 2021a. Hatchfrac: A fast open-source dfn modeling software. Earth and Space Science Open Archive , 44.

Zhu, W., Khirevich, S., Patzek, T.W., 2021b. Impact of fracture geometry and topology on the connectivity and flow properties of stochastic fracture networks. Water Resour. Res. , e2020WR028652.

Zhu, W., Lei, G., He, X., Patzek, T.W., Wang, M., 2022. Fractal and multi-fractal characterization of stochastic fracture networks and real outcrops. J. Struct. Geol. , 104508.

Zhu, W., Lei, G., He, X., Yang, Y., Santoso, R.K., Wang, M., 2021c. Are natural fractures pervasive? Earth and Space Science Open Archive , 46.